Journal of Marine Science and Technology

Volume 25 | Issue 1 Article 12

NUMERICAL SIMULATION OF SOLITARY WAVE PROPAGATION IN A VEGETATED CHANNEL USING AN EXTENDED BOUSSINESQ MODEL

Mingliang Zhang
School of Ocean Science and Environment, Dalian Ocean University, Dalian, Liaoning, PR China. State Key Laboratory of Hydraulics and Mountain River Engineering, Sichuan University, Chengdu, Sichuan, PR China.,
zhmliang_mail@126.com

Huiting Qiao
School of Ocean Science and Environment, Dalian Ocean University, Dalian, Liaoning, PR China.

Yuanyuan Xu
State Key Laboratory of Coastal and Offshore Engineering, Dalian University of Technology, Dalian, Liaoning, PR China.

NUMERICAL SIMULATION OF SOLITARY WAVE PROPAGATION IN A VEGETATED CHANNEL USING AN EXTENDED BOUSSINESQ MODEL

Acknowledgements

This work was supported by the National Nature Science Foundation of China (51579030), the Wetland Degradation and Ecological Restoration Program of Panjin Pink Beach (PHL-XZ-2017013002), the Liaoning Natural Science Foundation (2014020148), the Open Fund of the State Key Laboratory of Hydraulics and Mountain River Engineering (SKHL1517).

Journal of Marine Science and Technology, Vol. 25, No. 1, pp. 119-128 (2017)
DOI: 10.6119/JMST-016-1019-1

NUMERICAL SIMULATION OF SOLITARY WAVE PROPAGATION IN A VEGETATED CHANNEL USING AN EXTENDED BOUSSINESQ MODEL

Mingliang Zhang[1, 3], Huiting Qiao[1], and Yuanyuan Xu[2]

Key words: FD/FV method, extended Boussinesq equations, HLL scheme, vegetation effect, wave attenuation.

ABSTRACT

An explicit one-dimensional model based on the extended Boussinesq equations was established to calculate solitary wave propagation in vegetated and non-vegetated waters. This model adopts a hybrid solution combining the finite difference (FD) and the finite-volume (FV) methods. This hybrid model can also simulate wave propagation as the FV solution of a non-linear shallow water equations (NSWE) model by removing the higher order Boussinesq terms. The resistance force caused by vegetation is added into a source term in the momentum equation. The interface fluxes are evaluated using the Harten-Lax-van Leer (HLL) approximate Riemann solver with reconstruction technique, providing a robust method to track the moving shoreline. This model is used to simulate solitary wave run-up on a sloping bed with vegetation and to evaluate wave attenuation through a vegetation zone. It is found that the model reasonably predicts wave height attenuation in cases where there is combined vegetation in a flat bed, implying that vegetation may cause energy loss in solitary wave propagation. The larger wave height and the larger vegetation density cause the larger wave attenuation for solitary waves through vegetation water. A positive correlation is found between wave attenuation and wave height. Modeling vegetation through the use of a source term in momentum equations is proved to provide a reasonable estimation for the amount of wave height attenuation that may occur through wetland marshes.

Paper submitted 01/27/16; revised 05/31/16; accepted 10/19/16. Author for correspondence: Mingliang Zhang (e-mail: zhmliang_mail@126.com).
[1] School of Ocean Science and Environment, Dalian Ocean University, Dalian, Liaoning, PR China.
[2] State Key Laboratory of Coastal and Offshore Engineering, Dalian University of Technology, Dalian, Liaoning, PR China.
[3] State Key Laboratory of Hydraulics and Mountain River Engineering, Sichuan University, Chengdu, Sichuan, PR China.

I. INTRODUCTION

Different forms of coastal vegetation create coastal wetlands. Examples include mangrove forests, wetland reeds, marsh or seagrass growing in soil near coastal waters, and others. This wetland vegetation is regarded as a means of providing stabilization of banks, habitat and food for animals, and serveing as a pleasing landscape for recreational use (Irtem, 2009; Li and Zhang, 2010; Blackmar, 2014). Furthermore, healthy wetland vegetation can also function as a natural barrier against catastrophic typhoon or tsunamis by attenuating wave energy (Kathiresan, 2005; Sanchez-Gonzalez, 2011). Marine/estuarine vegetation, however, consists of complex leaf shapes, rigid and flexible properties, and variable plant types. As such, it is difficult to evaluate the effects of marine/estuarine vegetation on wave energy attenuation, and the wave-vegetation interaction processes are not well understood. With advances in computer technology and numerical methods, numerical simulations have become useful tools for studying the hydrodynamic processes of coastal waters, and are widely applied to help understand the interactions between waves and coastal aquatic vegetations.

Numerical methods can be classified into three groups: finite-difference method (FDM), finite-element method (FEM) and finite volume method (FVM). FVM coupled with nonlinear shallow water equations (NSWE) is a frequently applied model for simulating wave propagation, and can represent breaking waves as propagating bores or hydraulic jumps (Li, 2002). In the case of dealing with flow discontinuities, a proper treatment of the shoreline motions must be considered to accurately model wave run-ups for the shore's dry states. Godunov-type schemes based on a Riemann solver have remarkable shock-capturing capabilities, and can address discontinuous flows. They have been used to process breaking wave simulations, such as surf zone wave breaking. Researchers have applied shock-capturing finite volume schemes in both coastal and riverine flood hazard modeling (Dodd, 1998; Hu, 2000; Begnudelli, 2008; Kuiry, 2012). Although these applications are relevant to surf-zone processes in some aspects, the lack of dispersion in the nonlinear shallow-water equations hampers their application to nearshore wave modeling.

NSWE has good capacity for the nonlinear non-dispersive

transformation of broken-waves, represented as shocks, in the inner surf and swash zones. However, due to the absence of frequency dispersion, the NSWE can not be applied to wave propagation before breaking. When a wave is propagated from a distance far away from the shoreline, the dispersion effect is important and the NSWE is not suitable. Therefore, a set of dispersive and hyperbolic depth-averaged equations have been developed using a hyperbolic approximation of a set of fully nonlinear and weakly dispersive Boussinesq-type equations (Bellotti, 2002; Antuono, 2009; Grosso, 2010; Antuono, 2013; Brocchini, 2013). The extended Boussinesq formulations of Madsen and Sørensen (MS) and Nwogu (1993) have been widely applied to model wave propagation from deep to shallow water. Using this foundation, a number of studies have successfully verified models to solve Boussinesq equations with either field or laboratory data, and have yielded reasonable results in predicting different run-up features (Madsen, 1992; Shiach, 2009; Tonelli, 2010; Kazolea, 2013). In considering the drag force caused by wetland vegetation, an additional drag force sink term is implemented into the momentum equations. This approach has proven successful in representing the interaction of flow with submerged and emergent vegetation (Lopez and Garcia, 2001; Wilson, 2006; Iimura, 2012; Tang, 2013). A new analytical equation has been derived to convert the drag resistance induced by submerged vegetation into an equivalent Manning roughness coefficient (Zhang, 2013). Recently, the drag force approach is also applied to calculate the effects of regular and irregular waves through vegetation (Li and Zhang, 2010).

This paper investigates the propagation process of solitary waves crossing vegetation using the NSWE and extended Boussinesq models. The intercell fluxes of the models are evaluated using the HLL approximate Riemann solver with MUSCL (Monotonic Upstream Scheme for Conservation Laws) reconstruction, it can accurately capture the moving waterline and simulate multiple flow regimes, including subcritical, transcritical, or supercritical flows. The effects of vegetation on the flow are represented in momentum equations. The proposed model can be applied to both wet- and dry-shorelines and can be further used to model dam-break wave and solitary wave propagations with or without vegetation. The numerical model is verified against measured data, the results will be presented in next sections.

II. MATHEMATICAL MODEL

1. Governing Equation

The hybrid model used in this study is based on the extended Boussinesq equations of Madsen and Søensen (1992) and can be expressed as follows:

$$\frac{\partial \eta}{\partial t}+\frac{\partial (hu)}{\partial x}=0 \tag{1}$$

$$\frac{\partial (hu)}{\partial t}+\frac{\partial \left(hu^2\right)}{\partial x}=-gh\frac{\partial \eta}{\partial x}-gn^2u\left|u\right|h^{-1/3}-\frac{\partial \psi}{\partial x}-f \tag{2}$$

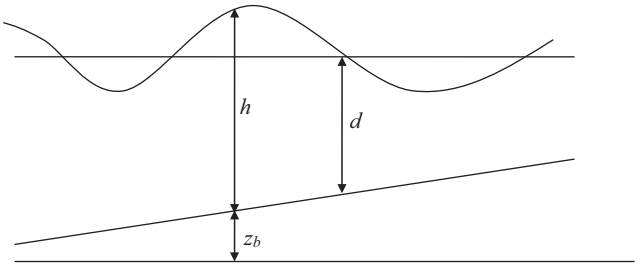

Fig. 1. Sketch of geometry and solution variables.

In these equations, t is the time, h is the flow depth, η is the water surface elevation ($\eta = h + z_b$) as shown in Fig.1. The variable z_b is the bed elevation in Fig. 1, u is the depth-averaged velocity, n is the Manning roughness coefficient, g is the gravitational acceleration, and f is the vegetation effect force on the wave.

$$\begin{aligned}\frac{\partial \psi}{\partial x}=&-\left(B+\frac{1}{3}\right)d^2\left(\frac{\partial^3 (hu)}{\partial x^2\partial t}\right)\\&+Bgd^3\frac{\partial^3\eta}{\partial x^3}-d\frac{\partial d}{\partial x}\left(\frac{1}{3}\frac{\partial^2 (hu)}{\partial x\partial t}+2Bgd\frac{\partial^2\eta}{\partial x^2}\right)\end{aligned} \tag{3}$$

In this equation, ψ is the model dispersion term, B represents the Boussinesq linear dispersion enhancement coefficient with a value of 1/15, and d is the still water depth from bed to still water level (SWL).

A one-dimensional form of the extended Boussinesq equations is rewritten in vector form:

$$\mathbf{D}\mathbf{U}_t+\mathbf{F}_x=\mathbf{S} \tag{4}$$

In Eq. (4), **U**, **F**(U) and **S**(U) are the vectors of conserved variables, fluxes, and source term in the x direction, respectively, defined as follows:

$$\begin{aligned}\mathbf{D}=&\begin{bmatrix}1&0\\0&1\end{bmatrix},\ \mathbf{U}=\begin{bmatrix}h\\ \mathrm{U}(hu)\end{bmatrix},\ \mathbf{F}\\&=\begin{bmatrix}hu\\ huu\end{bmatrix},\ \mathbf{S}=\begin{bmatrix}0\\ gh\dfrac{\partial\eta}{\partial x}-gn^2u\left|u\right|h^{-1/3}-f+s_d\end{bmatrix}\end{aligned} \tag{5}$$

In this equation, U(hu) is the velocity function, S_d is dispersion term.

For the extended Boussinesq equation,

$$\mathrm{U}(hu)=hu-(B+\frac{1}{3})d^2\frac{\partial^2(hu)}{\partial x^2}-\frac{1}{3}d\frac{\partial d}{\partial x}\frac{\partial (hu)}{\partial x},$$

$$\mathrm{s}_d=Bgd^3\frac{\partial^3\eta}{\partial x^3}+2Bgd^2\frac{\partial d}{\partial x}\frac{\partial^2\eta}{\partial x^2} \tag{6}$$

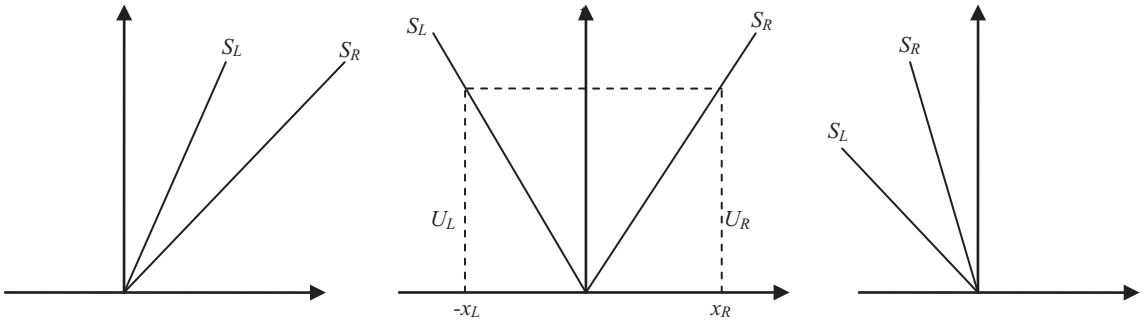

Fig. 2. Three possible wave configurations.

For the nonlinear shallow water equation,

$$\mathrm{U}(hu) = hu,\ S_d = 0 \tag{7}$$

2. Numerical Scheme

1) Spatial Discretisation and Time Integration

The numerical scheme used to solve the governing equations is a fourth-order in space, second-order accurate in time, and uses the hybrid FD and FV scheme. The flux terms are discretised using a finite-volume method; the pressure source term of water level and dispersion term (S_d) are discretised using centered finite-differences (Shiach, 2009; Tonelli, 2010).

The extended Boussinesq equations can be integrated at a control volume:

$$\int_\Omega \mathbf{D}\frac{\partial \mathbf{U}}{\partial t} + \int_\Omega \frac{\partial \mathbf{F}}{\partial x} d\Omega = \int_\Omega \mathbf{S} d\Omega \tag{8}$$

Time integration is performed using a predictor-corrector scheme, which is second order accurate in time (Shiach, 2009). The predictor step uses a non-conservative approach to determine the intermediate values over a half time step:

$$\mathbf{U}_i^{t+1/2} = \mathbf{U}_i^t - \frac{\Delta t}{2\Delta x_i}\left[\sum_{i=1}^{M} \mathbf{F}(\mathrm{U}_i)^t \cdot \mathbf{n}_i\right] \tag{9}$$

where t and $t + 1/2$ denote the current and intermediate values, Δx_i is the space step for cell i, M is the number of the cell sides, $\mathbf{n}_i$ is the outward pointing normal vector to side i and Δt is the time step.

The corrector step that provides the fully conservative solution over one time step is given by:

$$\begin{aligned}\mathbf{U}_i^{t+1} = \mathbf{U}_i^t &- \frac{\Delta t}{\Delta x_i}\left[\sum_{i=1}^{M} \mathbf{F}(\mathrm{U}_i^{\mathrm{L}}, \mathrm{U}_i^{\mathrm{R}})^{t+1/2} \cdot \mathbf{n}_i\right] \\ &+ \Delta t\left[gh\Delta\eta_i - gn^2 u|u|h^{-1/3} - f + \mathrm{S}_d\right]\end{aligned} \tag{10}$$

where $\mathbf{F}(\mathrm{U}_i^{\mathrm{L}}, \mathrm{U}_i^{\mathrm{R}})^{t+1/2}$ is the flux vector function of the predictor step at the cell interface i, the values are found by solving a local Riemann problem that occurs at each interface. Variables $\mathbf{U}_i^{\mathrm{L}}$ and $\mathbf{U}_i^{\mathrm{R}}$ are the values of the conserved variables to the left- and right-hand side of cell boundaries.

A variable Δt is needed to require a Courant-Friedrichs-Lewy (CFL) condition for an explicit scheme model. The one dimensional solver is:

$$\Delta t = \nu \min\left(\frac{\Delta x_i}{|u_i| + \sqrt{gh_i}}\right) \tag{11}$$

Here, ν is Courant number between zero and one, ν is recommended with a value 0.7 in this study.

2) Riemann Fluxes

A detailed description of the HLL scheme are provided by Toro (2001) and Zhang (2012), which include a detailed discussion about the Riemann problem and the reasons for a special treatment of the cells on the wave front or shore line (wet/dry boundary). The HLL scheme assumes only one constant intermediate state between the left and the right wave, as shown in Fig. 2.

The HLL scheme assumes and defines the flux at an interface as

$$\mathbf{F}_{\mathrm{HLL}} = \begin{cases} \mathbf{F}_{\mathrm{L}} & if\ \mathrm{S}_{\mathrm{L}} \geq 0 \\ \mathbf{F}^* & if\ \mathrm{S}_{\mathrm{L}} < 0 < \mathrm{S}_{\mathrm{R}} \\ \mathbf{F}_{\mathrm{R}} & if\ \mathrm{S}_{\mathrm{R}} \leq 0 \end{cases} \tag{12}$$

In this scheme, $\mathbf{F}_{\mathrm{L}}$ and $\mathbf{F}_{\mathbf{R}}$ are the flux evaluated at the left-hand and the right-hand sides of each cell interface. In the model, the HLL approach provides the approximate expression for estimating **F***

$$\mathrm{F}^* = \frac{\mathrm{S}_{\mathrm{R}}\mathrm{F}_{\mathrm{L}} - \mathrm{S}_{\mathrm{L}}\mathrm{F}_{\mathrm{R}} + \mathrm{S}_{\mathrm{L}}\mathrm{S}_{\mathrm{R}}\left(\mathrm{U}_{\mathrm{R}} - \mathrm{U}_{\mathrm{L}}\right)}{\mathrm{S}_{\mathrm{R}} - \mathrm{S}_{\mathrm{L}}} \tag{13}$$

In this equation, the symbols S_L and S_R represent the wave celerity, separating constant states of the local Riemann problem solution at cell interfaces.

The symbols S_L and S_R can be estimated as follows:

$$S_L = \min\left(U_L - \sqrt{gh_L}, u^* - \sqrt{gh^*}\right) \tag{14}$$

$$S_R = \max\left(U_R + \sqrt{gh_R}, u^* + \sqrt{gh^*}\right) \tag{15}$$

$$u^* = \frac{1}{2}\left(U_L + U_R\right) + \sqrt{gh_L} - \sqrt{gh_R} \tag{16}$$

$$\sqrt{gh^*} = \frac{1}{2}\left(\sqrt{gh_L} + \sqrt{gh_R}\right) + \frac{1}{4}\left(U_L - U_R\right) \tag{17}$$

The symbols h_L and h_R are the water depth of the left and right states. For a dry bed problem the wave speeds S_L and S_R are estimated according to the following expressions:

$$S_L = U_L - \sqrt{gh_L},\ S_R = U_L + 2\sqrt{gh_L} \tag{18}$$

for right dry bed

$$S_L = U_R - 2\sqrt{gh_R},\ S_R = U_R + \sqrt{gh_R} \tag{19}$$

for left dry bed

If the intermediate states U_L and U_R are defined as the cell-centered values, a first-order accurate scheme is obtained, which suffers from excess numerical dissipation, limiting accuracy. A fourth-order MUSCL reconstruction is first used to calculate interface values in the Navier-Stokes solver by Yamamoto et al. (1998). In this study, the technique is used to reduce the model's truncation errors of dispersion terms. Usually, a van Leer nonlinear slope limiter function is used to calculate the interfaces fluxes at the cell in x direction, the minmod slope limiter is used here to eliminate under/overshoots that caused spurious oscillations in the solution.

3) Evaluation of Velocity Function

The velocity function can be discretized using a finite difference scheme and can be rewritten using the matrix equation for the extended Boussinesq equations:

$$\mathrm{U}(hu)_i = a_i\left(hu\right)_{i-1} + b_i\left(hu\right)_i + c_i\left(hu\right)_{i+1} \tag{20}$$

Therefore, the coefficients of diagonal elements for Madsen and Sørensen's formulation are:

$$a_i = -\frac{\left(B + 1/3\right)d_i^2}{\Delta x_i^{\,2}} + \frac{d_i}{12\Delta x_i^{\,2}}\left(-d_{i-1} + d_{i+1}\right) \tag{21}$$

$$b_i = 1 + \frac{2\left(B + 1/3\right)d_i^2}{\Delta x_i^{\,2}} \tag{22}$$

$$c_i = -\frac{\left(B + 1/3\right)d_i^2}{\Delta x_i^{\,2}} - \frac{d_i}{12\Delta x_i^{\,2}}\left(-d_{i-1} + d_{i+1}\right) \tag{23}$$

The tri-diagonal system can be calculated to obtain the U(hu) value by applying the Thomas algorithm after the predictor and corrector stages (Bellotti, 2002; Shiach, 2009).

4) Evaluation of Dispersion Term

The spatial derivatives present in the dispersion term are discretised using central difference, and are expressed as follows:

$$\begin{aligned} \mathrm{s}_d = {} & \frac{Bgd_i^3}{2\Delta x_i^{\,3}}\left(-\eta_{i-2} + 2\eta_{i-1} - 2\eta_{i+1} + \eta_{i+2}\right) \\ & + \frac{Bgd_i^2}{2\Delta x_i^{\,3}}\left(d_{i-2} - 8d_{i-1} + 8d_{i+1} - d_{i+2}\right)\left(\eta_{i-1} - 2\eta_i + \eta_{i+1}\right) \end{aligned} \tag{24}$$

3. Resistance of Vegetation on Waves

The effect of vegetation on waves can be simulated using an internal source of resistant force per unit fluid mass added into the momentum equations; the resistance force exerted on vegetation per unit volume can be expressed as (Li and Zhang, 2010):

$$\begin{aligned} f = Nf_D + Nf_I = {} & \frac{1}{2}NC_D b_v \min(h_v, h)u\left|u\right| \\ & + NC_M b_v t_v \min(h_v, h)\frac{\partial u}{\partial t} \end{aligned} \tag{25}$$

In this equation, where f_D is the drag force, f_I is the inertia force, C_D is the drag force coefficient, N is the vegetation density defined as the number of vegetation elements per unit area, b_v and t_v are the width and thickness of a vegetation element, respectively. h_v is the height of vegetation, and C_M is the inertia force coefficient.

III. APPLICATION OF MODEL

1. Dam-Break Flow at a Sloping Bed

The first test validated the simulation accuracy of the NSWE model. The laboratory dam-break flow on a sloping beach was recommended by Aureli (2000). The physical experiment included complex hydraulic properties such as run-up and rundown between wet and dry beds. The laboratory set up is illustrated in Fig. 3. The rectangular channel for this experiment is 7 m in length; the experiment consists of a reservoir with water depth up to 0.25 m, contained by a dam at x = 2.25 m, and a dry bed downstream. The 1:10 sloping beach is located at 1.25 m downstream of the dam. To observe the depth evolutions, all gauges are located at 1.4 m, 2.25 m, 3.4 m, and 4.5 m from the upstream boundary, as shown in Fig. 3. The Manning roughness coefficient is set as 0.01 s $\cdot$ m$^{-1/3}$ with the same value of the experiment. In the computation, Δx = 0.1 m, Δt = 0.001 s, the

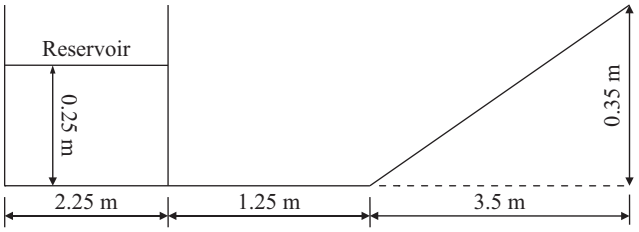

Fig. 3. Layout of the dam-break experiment (Aureli, 2000).

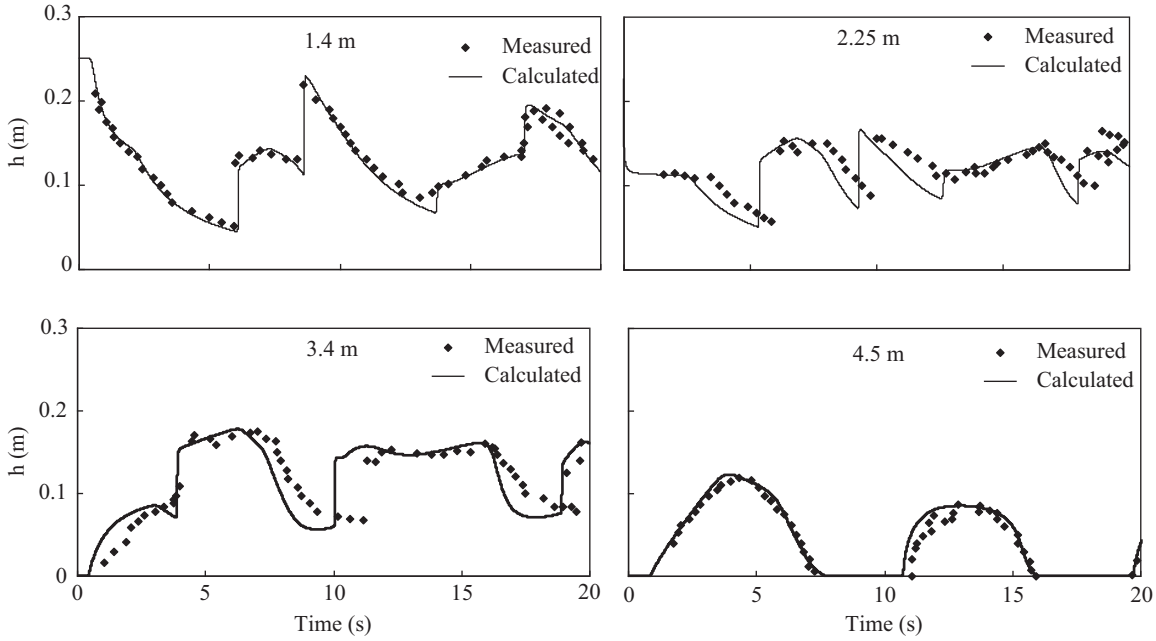

Fig. 4. Comparison of simulated water depths and experimental data.

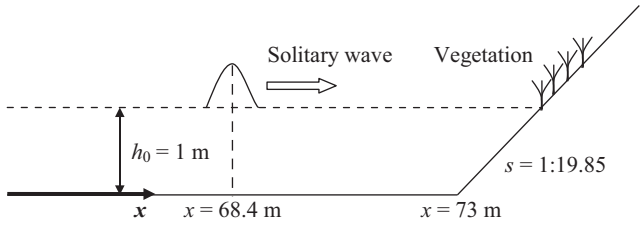

Fig. 5. Sketch of the solitary wave run-up on a sloping beach.

simulation was carried out for 20 s. The calculated water depth time series at the four gauge points are shown in Fig. 4. This shows that the predicted water depth evolutions and arrival time of the wave are comparable and in agreement with the measured data at all gauges. At time $t = 0$, the dam is removed suddenly, and the reservoir water floods downstream due to gravity. When it reaches the sloping beach, the flooding wave begins to run up and is then partially reflected, generating a wave propagating upstream. The run-up and rundown processes repeat several times until balance is reached due to bed friction. The calculated results show that the NWSE model has capability to simulate the dam-break wave process.

2. Solitary Wave Run-up and Reflection at a Sloping Beach

Solitary wave propagation in shallow water, and associated processes such as wave-breaking and run-up played an important role in the nearshore dynamics, so solitary wave run-up on a sloping beach was one of the most intensively studied problems in long-wave modeling. Laboratory experiments carried out by Synolakis (1986) provide important data for validation tests in wave-breaking and run-up modeling, as shown in Fig. 5. In Synolakis's experiment, the constant water depth was 1 m, and a solitary wave of height was 0.3 m, propagating from left to right on a 1:19.85 sloping beach. In our study, the NSWE model and the extended Boussinesq model were used to reproduce the wave propagation processes in Synolakis's experiment. The initial conditions include a solitary wave, propagating from left to right, with the wave crest located at X_1. The initial solitary wave is simulated by the solitary wave formula as (Kuiry, 2012):

$$\eta(x,0) = H \sec h^2\left(\sqrt{(3H/(4d))}\,(x - X_1)\right) \qquad (26)$$

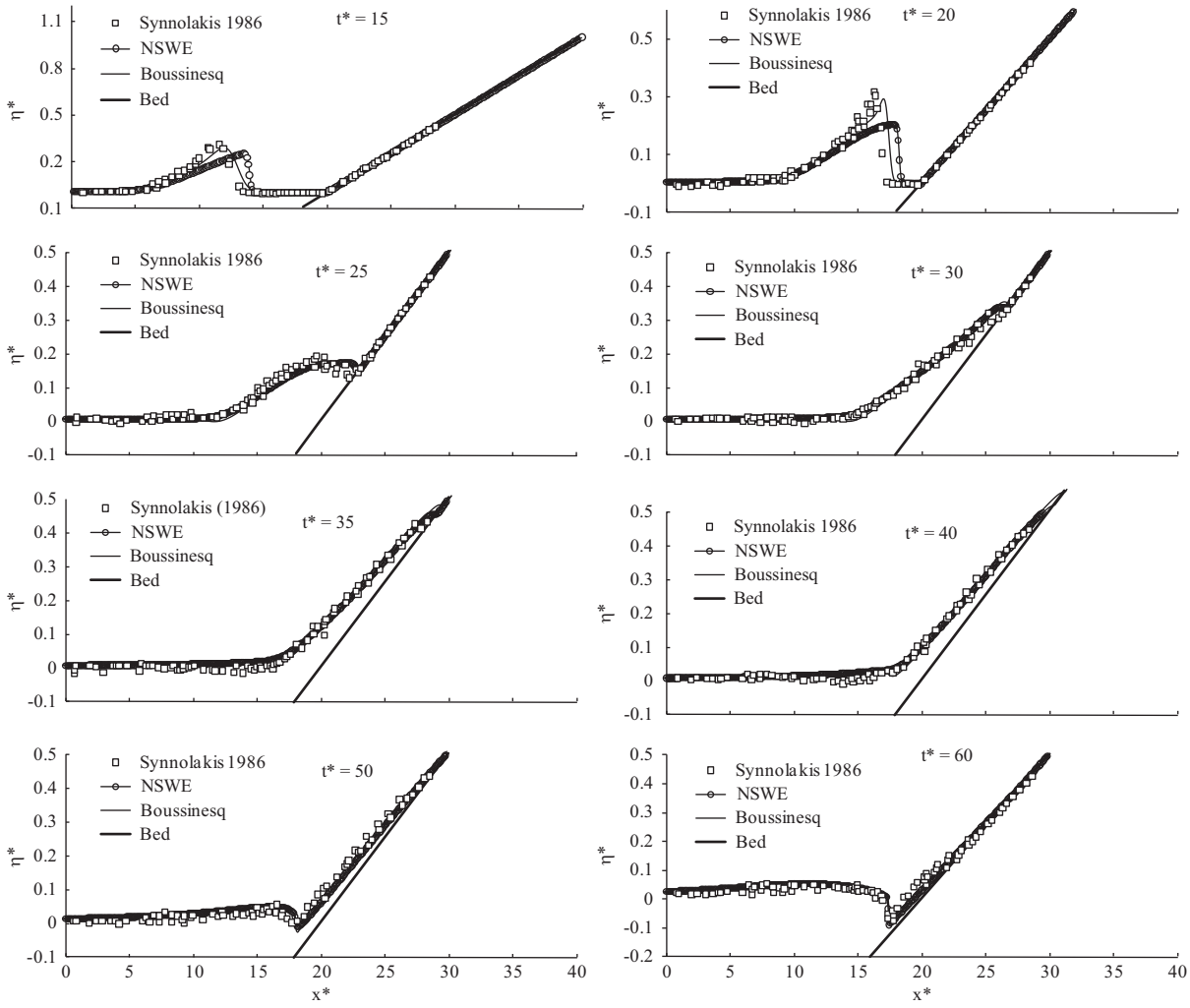

Fig. 6. Comparison of solitary wave run-up and rundown on a 1:19.85 sloping beach.

$$u(x,0)=\sqrt{\frac{g}{d}}\eta(x,0) \tag{27}$$

In these equations, H is initial wave height of the solitary wave.

The computation domain is subdivided into cells in a uniform mesh with space step Δx = 0.1 m; the Manning coefficient is 0.01. Simulated results of water surface profiles are recorded to provide a comparison with the experimental data. Fig. 6 compares the measured and computed wave profiles; the water surface elevation and the length scale are normalized by the water depth, $x^* = (x - x_{toe})/d$, x_{toe} is the initial location of slope's toe; and the time scale is normalized as $t^* = t\sqrt{g/d}$. As seen in this figure, as the initially symmetric solitary wave shoals across the slope's toe at x = 73 m, the wave speed is slowed by the bottom friction and the seabed's topography. As such, it begins to skew to the front forming a vertically-faced propagating bore. To simulate the long wave run-up on beaches, the numerical model must correctly reproduce the run-up process and the highest climb-up of the water front. In this study, both the NSWE model and the Boussinesq model accurately present the run-up process as shown Fig. 6. The obtained results using the NSWE model do have some discrepancies at the wave crest compared to the experimental data, particularly with respect to simulating the breaking zone wave profile. Those discrepancies may be due to the limitation of the shallow water equation itself in simulating wave dispersion. Overall, the extended Boussinesq system provides wave transformation results at higher accuracy levels, particularly with respect to the breaking zone wave profile, and the accurate wave rundown processes from the sloping beach can be also presented. In next cases, the extended Boussinesq model will be further tested owing to its capability of calculating breaking waves.

3. Solitary Wave Propagation on a Flat Bed with Emergent Vegetation

In this study, we investigated the interactions of solitary waves with emergent vegetation on a flat bed using the extended Boussinesq model. The cases were from the laboratory experiments

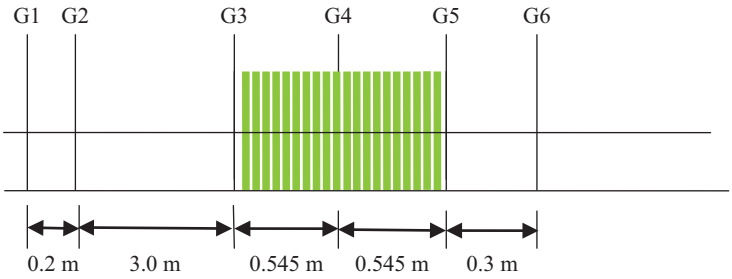

Fig. 7. Locations of wave probes and vegetation arrangement for model B2.

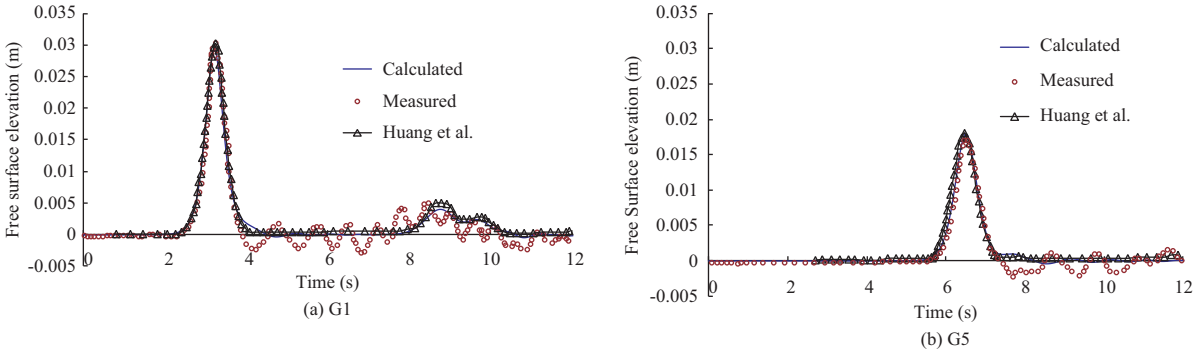

Fig. 8. Comparison of calculated water surface elevations above SWL for model B2.

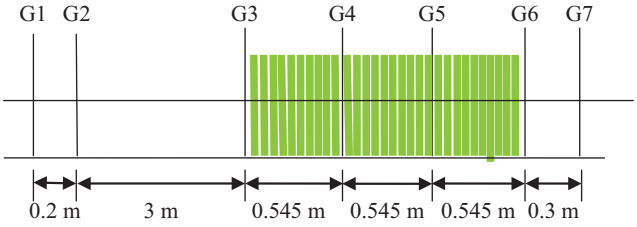

Fig. 9. Locations of wave probes and vegetation arrangement for model C3.

conducted by Huang et al. (2011), the glass-walled wave flume was 32 m long and 0.55 m wide. The vegetation models were placed on the horizontal bed in the middle of the wave flume. The model vegetation was made of Perspex tubes with a uniform outer diameter of 0.01 m; each vegetation block was 0.545 m in width. Experiments B2 had a solid volume portion of 0.087, which could be recalculated to vegetation density per unit area; six resistance-type wave probes were used to record the surface elevations at the selected locations, as shown in Fig. 7. The initial water depth was 0.15 m, the incident wave height was 0.03 m. The computational domain was represented with a mesh consisting of 2500 cells in the longitudinal direction; the space step was 0.02 m in this study. The time step was variable and determined using the CFL stability condition. The Manning roughness coefficient n was 0.01. The drag coefficient C_D and the initial drag coefficient C_M were calibrated as bulk constants of 1.45 and 2.0, respectively.

Fig. 8 shows the comparison of the predicted and measured water surface elevation above SWL for G1 and G5 stations, the calculated results follow closely with the measured data. Slight discrepancies can be found in the evolution of undulating tails; these weaker undulating tails were also predicted by other researchers using different numerical schemes, the computed main peaks and shapes of the waves follow the measured ones very well, except for the details in the undulating tails (Huang, 2011). The calculated water surface elevation above SWL was 0.03 m in front of the vegetation block (G1) and the calculated water surface elevation above SWL decreased to 0.017 m behind the vegetation block (G5). The vegetation obviously influenced the wave propagation. Experiments C3 has a solid volume portion of 0.044; seven resistance-type wave probes were used to record the surface elevations above the still water depth at the selected locations, as shown in Fig. 9. The incident wave height is 0.05 m. The drag coefficient C_D and the initial drag coefficient C_M in this case are calibrated as bulk constants of 1.45 and 2.0, respectively (Huang et al., 2011).

Comparing the numerical and experimental data reveals that the simulated results show a good level of accuracy against the measured data considering the vegetation effect, as shown in Fig. 10. In experiment B2, γ stands for the ratio of wave height attenuation, $\gamma = (\eta_{G1} - \eta_{G5})/\eta_{G1} = 43\%$; in experiment C3, $\gamma = (\eta_{G1} - \eta_{G5})/\eta_{G1} = 27\%$, when the vegetation density increases, the water surface elevation above SWL decreases more quickly at the same length in the vegetation domain. Fig. 11 shows an approximate linear relationship between the wave surface elevation reduction and the vegetation width. The attenuation of

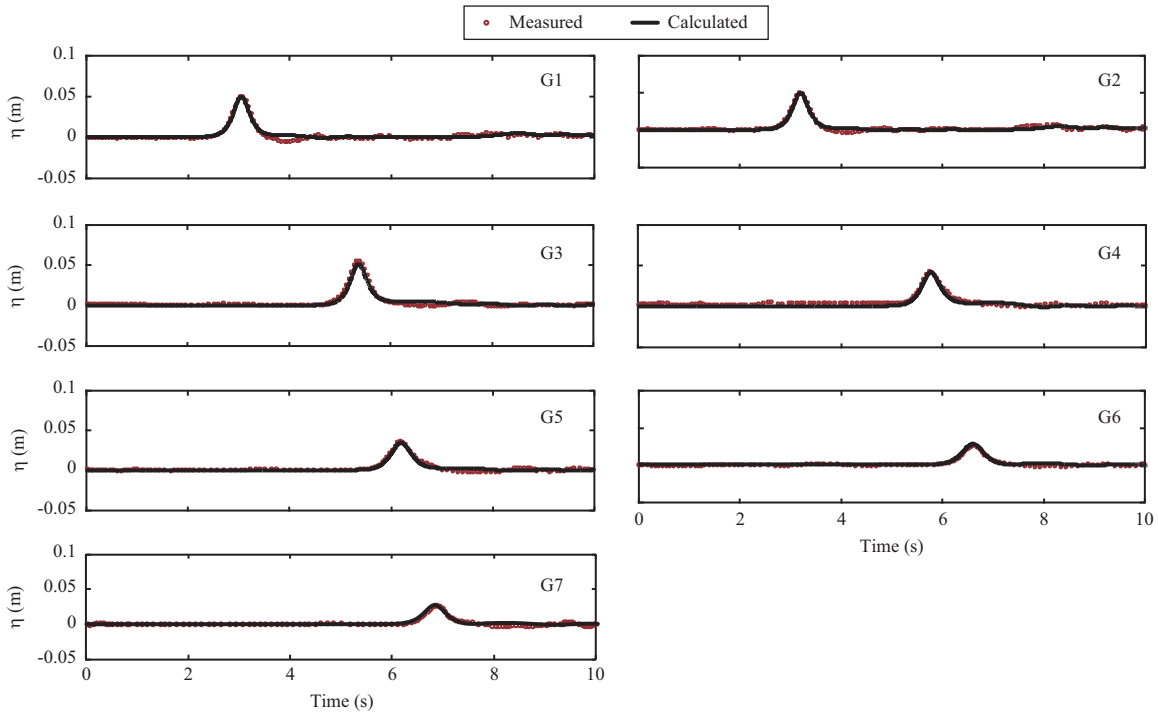

Fig. 10. Comparison of calculated water surface elevations above SWL at different locations for model C3.

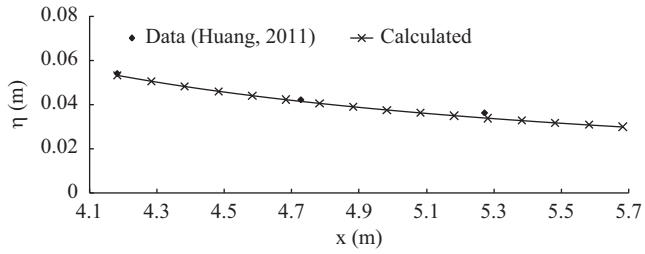

Fig. 11. Linear relationship between the water surface elevations above SWL and the width of vegetation for model C3.

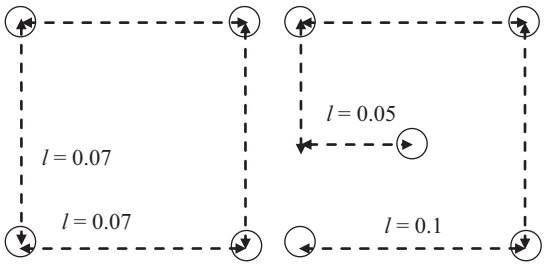

Fig. 13. Vegetation arrangement used in this study.

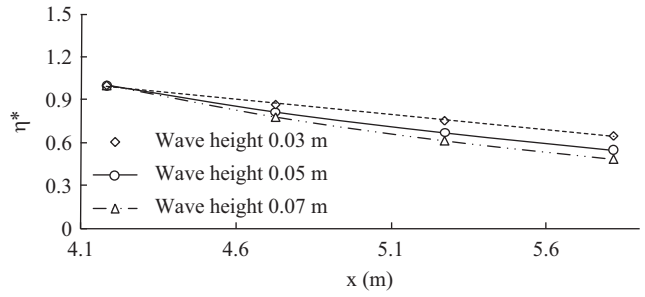

Fig. 12. Water surface elevation attenuation over vegetation with different incident wave heights for model C3.

water surface elevation along the channel with varying incident wave heights is shown in Fig. 12. The results report the water surface elevation above SWL normalized by the incident wave heights. It can be seen that the larger wave height causes the larger attenuation of water surface elevation at the same vegetation zone. These findings should be further explored in the future using more experimental data across different vegetation types.

4. Solitary Wave Run-Up and Reflection at a Sloping Beach with Vegetation

Coastal areas are often affected by typhoons and tsunamis. Where disasters occur frequently (for example damage of coastal levees), one of main causes of damage is the impact of waves on levees. In recent years, biological revetment form (planting vegetation on beaches) has already began to be used to reduce wave energy, but detailed wave-vegetation interactions on sloping beaches needs further study. In this case, the extended Boussinesq model with one-dimensional form was used to investigate the solitary wave run-up and the solitary wave energy attenuation in vegetated and non-vegetated channel. The detailed calculation domain and the vegetation arrangements are shown in Fig. 5 and Fig. 13, the diameter of the plants was 0.01 m, the plant height was 0.3 m, the density was 200 and 400 plants per

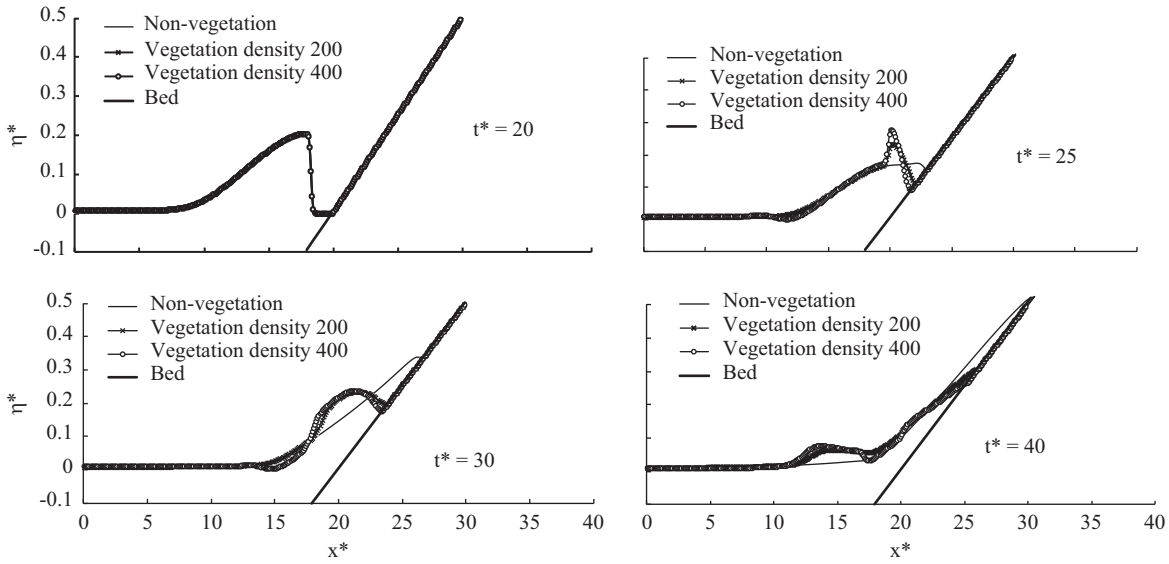

Fig. 14. Comparison of the solitary wave run-up and rundown with and without vegetation.

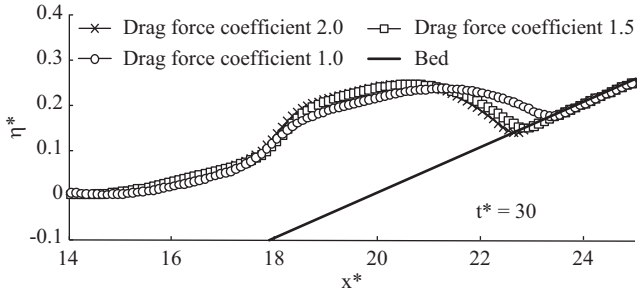

Fig. 15. Comparison of the solitary wave run-up with the different coefficients of C_D.

unit area for different arrangement, and the plant length was 0.3 m. Fig. 14 shows the comparison of solitary wave run-up and run-down with and without vegetation. In Fig. 14, when $t^* = 20$, the calculated water level of vegetated and non-vegetated conditions almost coincide, the main reason for this coincidence is that the solitary wave movement has not reached the vegetation zone, and therefore, the wave propagation is not affected by plants. When $t^* = 25$, $t^* = 30$ and $t^* = 40$, the run-up height of the solitary wave in the presence of vegetation is lower than that in the absence of vegetation; solitary waves propagating through vegetation lose energy due to their interaction with the vegetation. The propagation of the solitary wave is discussed along the channel with varying drag coefficients shown in Fig 15. It can be seen that larger vegetation drag force and vegetation densities cause larger wave attenuation. The model was able to reproduce the effect of breaking solitary waves dampened by vegetation over a sloping beach, and the results show that the vegetation field damping should be considered to be a biological mechanism to reduce typhoon and tsunami damage.

IV. CONCLUSION

In this study, we used a hybrid FV/FD scheme of 1D extended Boussinesq model to simulate the wave propagation through vegetated and non-vegetated waters. The HLL solver was used to calculate the flux of interface by using fourth-order MUSCL reconstruction for left and right interfaces. The vegetation field was represented by an additional sink term in the momentum equation. The model was validated using several cases, including dam-break wave and solitary wave propagation on vegetated and non-vegetated channels. We paid special attention to compare the results of the Boussinesq model and the NSWE model. The calculated results show that the extended Boussinesq model presents more accurate results than the NSWE model due to the dissipative terms in the wave breaking process. The model solutions, however, are almost identical in run-up and rundown processes after wave breaking. For the vegetated sloping beach, the calculated results from the extended Boussinesq model show that the solitary wave run-up height decreases quickly and wave rundown processes occur in advance, due to the effect force of vegetation on waves. The simulated results show that planting wetland vegetation on a coastal bank may be effective in reducing wave energy and reducing disasters caused by typhoons or tsunamis. The developed Boussinesq model can be used to forecast the effect of vegetation on typhoon and tsunami wave propagation, and provide guidance on riparian vegetation management for coastal wetland waters.

ACKNOWLEDGEMENTS

This work was supported by the National Nature Science Foundation of China (51579030), the Wetland Degradation and Ecological Restoration Program of Panjin Pink Beach

(PHL-XZ-2017013002), the Liaoning Natural Science Foundation (2014020148), the Open Fund of the State Key Laboratory of Hydraulics and Mountain River Engineering (SKHL1517).

REFERENCES

Antuono, M., V. Liapidevskii and M. Brocchini (2009). Dispersive nonlinear shallow water equations. Studies in Applied Mathematics 122(1), 1-28.

Antuono, M. and M. Brocchini (2013). Beyond Boussinesq-type equations: Semi-Integrated models for coastal dynamics. Physics of Fluids 25, 016603.

Augustin, L. N., J. L. Irish and P. Lynett (2009). Laboratory and numerical studies of wave damping by emergent and near-emergent wetland vegetation. Coastal Engineering 56, 332-340.

Aureli, F., P. Mignosa and M. Tomirotti (2000). Numerical simulation and experimental verification of dam break flows with shocks. Journal of Hydraulic Research 38(3), 197-206.

Begnudelli, L., B. F. Sanders and S. F. Bradford (2008). Adaptive Godunov-based model for flood simulation. Journal of Hydraulic Engineering 134 (6), 714-725.

Bellotti, G. and M. Brocchini (2002). On using Boussinesq-type equations near the shoreline: a note of caution. Ocean Engineering 29, 1569-1575.

Blackmar, P. J., D. T. Cox and W. C. Wu (2014). Laboratory observations and numerical simulations of wave height attenuation in heterogeneous vegetation. Journal of Waterway, Port, Coastal, and Ocean Engineering 140(1), 56-65.

Brocchini, M. (2013). A reasoned overview on Boussinesq-type models: the interplay between physics, mathematics and numerics. Proceedings of the Royal Society A 469, 1-27.

Dodd, N. (1998). Numerical model of wave run-up, overtopping, and regeneration. Journal of Waterway, Port, Coastal and Ocean Engineering 124 (2), 73-81.

Grosso, G., M. Antuono and M. Brocchini (2010). Dispersive nonlinear shallow water equations: Some numerical results. Journal of Engineering Mathematics 67(1-2), 71-84.

Hu, K., C. G. Mingham and D. M. Causon (2000). Numerical simulation of wave overtopping of coastal structures using the nonlinear shallow-water equations. Coastal Engineering 41, 433-465.

Huang, Z. H., Y. Yao, S. Y. Sim and Y. Yao (2011). Interaction of solitary waves with emergent, rigid vegetation. Ocean Engineering 38, 1080-1088.

Iimura, K. and N. Tanaka (2012). Numerical simulation estimating effects of tree density distribution in coastal forest on tsunami mitigation. Ocean Engineering 54, 223-232.

Irtem, E., N. Gedik, M. S. Kabdasli and N. E. Yasa (2009). Coastal forest effects on tsunami run-up heights. Ocean Engineering 36(3-4), 313-320.

Kathiresan, K. and N. Rajendran (2005). Coastal mangrove forests mitigated tsunami. Estuarine, Coastal and Shelf Science 65 (3), 601-606.

Kazolea, M., A. I. Delis and N. A. Kampanis (2013). A well-balanced shock-capturing hybrid finite volume-finite difference numerical scheme for extended 1D Boussinesq models. Applied Numerical Mathematics, 67, 167-186.

Kuiry, S. N., W. M. Wu and Y. Ding (2012). A one-dimensional shock-capturing model for long wave run-up on sloping beaches. Journal of Hydraulic Engineering 18(2), 65-79.

Li, C. W. and M. L. Zhang (2010). 3D modelling of hydrodynamics and mixing in a vegetation field under waves. Computers & Fluids 39, 604-614.

Li, Y. and F. Raichlen (2002). Non-breaking and breaking solitary wave run-up. Journal of Fluid Mechanics 456, 295-318.

López, F. and M. H. García (2001). Mean flow and turbulence structure of open channel flow through non-emergent vegetation. Journal of Hydraulic Enginering 127 (5), 392-402.

Madsen, P. A. and O. R. Sørensen (1992). A new form of the Boussinesq equations with improved linear dispersion characteristics. Part 2. A slowly-varying bathymetry. Coastal Engineering 18, 183-204.

Nwogu, O. (1993). Alternative form of Boussinesq equations for nearshore wave propagation. Journal of Waterway, Port, Coastal and Ocean Engineering 119(6), 618-638

Sanchez-Gonzalez, J. F., V. Sanchez-Rojas and C. D. Memos (2011). Wave attenuation due to Posidonia oceanica meadows. Journal of Hydraulic Research 49(4SI), 503-514.

Shiach, J. B. and C. G. Mingham (2009). A temporally second-order accurate Godunov-type scheme for solving the extended Boussinesq equations. Coastal Engineering 56, 32-45.

Synolakis, C. E. (1986). The run-up of long waves. Ph.D. Thesis, California Institute of Technology, Pasadena, CA.

Tang, J., D. Causon, C. Mingham and L. Qian (2013). Numerical study of vegetation damping effects on solitary wave run-up using the nonlinear shallow water equations. Coastal Engineering 75, 21-28.

Tonelli, M. and M. Petti (2010). Finite volume scheme for the solution of 2D extended Boussinesq equations in the surf zone. Ocean Engineering 37, 567-582.

Toro, E. F. (2001). Shock-capturing methods for free-surface shallow flows. England, Wiley.

Wilson, C. A. M. E., O. Yagci, H. P. Rauch and N. R. B. Olsen (2006). 3D numerical modelling of a willow vegetated river/floodplain system. Journal of Hydrology 327, 13-21.

Yamamoto, S., S. Kano and H. Daiguji (1998). An efficient CFD approach for simulating unsteady hypersonic shock–shock interference flows. Computers & Fluids 27 (5-6), 571-580.

Zhang, M. L., C. W. Li and Y. M. Shen (2013). Depth-averaged modeling of free surface flows in open channels with emerged and submerged vegetation. Applied Mathematical Modelling 37, 540-553.

Zhang, M. L., W. M. Wu, L. H. Lin and J. N. Yu (2012). Coupling of wave and current numerical model with unstructured quadtree grid for nearshore coastal waters. Science China Technological Sciences 55(2), 568-580.